PAPER

Microscopic deformation mechanism and main influencing factors of carbon nanotube coated graphene foams under uniaxial compression

View the article online for updates and enhancements.

Microscopic deformation mechanism and main influencing factors of carbon nanotube coated graphene foams under uniaxial compression

Shuai Wang[1,2] ⓘ**, Chao Wang**[3,4,*] ⓘ**, Muhammad Bilal Khan**[1,2] ⓘ **and Shaohua Chen**[1,2,*] ⓘ

[1] Institute of Advanced Structure Technology, Beijing Institute of Technology, Beijing, 100081, People's Republic of China
[2] Beijing Key Laboratory of Lightweight Multi-Functional Composite Materials and Structures, Beijing Institute of Technology, Beijing, 100081, People's Republic of China
[3] LNM, Institute of Mechanics, Chinese Academy of Sciences, Beijing, 100190, People's Republic of China
[4] School of Engineering Science, University of Chinese Academy of Sciences, Beijing, 100049, People's Republic of China

E-mail: wangchao@lnm.imech.ac.cn and chenshaohua72@hotmail.com

CrossMark

Abstract

Many experiments have shown that carbon nanotube-coated (CNT-coated) graphene foam (CCGF) has specific mechanical properties, which further expand the application of graphene foam materials in many advanced fields. To reveal the microscopic deformation mechanism of CCGF under uniaxial compression and the main factors affecting their mechanical properties, numerical experiments based on the coarse-grained molecular dynamics method are systematically carried out in this paper. It is found that the relative stiffness of CNTs and graphene flakes seriously affects the microscopic deformation mechanism and strain distribution in CCGFs. The bar reinforcing mechanism will dominate the microstructural deformation in CCGFs composed of relatively soft graphene flakes, while the microstructural deformation in those composed of stiff graphene flakes will be dominated by the mechanical locking mechanism. The effects of CNT fraction, distribution of CNTs on graphene flakes, the thickness of graphene flakes, and the adhesion strength between CNTs and graphene flakes on the initial and intermediate moduli of foam materials are further studied in detail. The results of this paper should be helpful for a deep understanding of the mechanical properties of CCGF materials and the optimization design of microstructures in advanced graphene-based composites.

Supplementary material for this article is available online

1. Introduction

The carbon nanotube-coated (CNT-coated) graphene foam (CCGF) is a new nanoporous composite material composed of the well-known one-dimensional CNTs [1] and two-dimensional

* Authors to whom any correspondence should be addressed.

graphene flakes [2], which inherits the unique structural and physicochemical properties [3, 4] of both CNT and graphene, and further obtains intrinsic synergistic effects of these two carbon materials. As a result, the CCGF has more outstanding mechanical [5–9] and electrical [10] properties, compared with its counterparts of pure CNT foams [11] and graphene foams [12] (GFs), which enables many practical applications in the field of sensing [13], energy storage devices [14], flexible electronics [15, 16], and damping materials [17] in recent years.

The mechanical properties of such a promising material are mainly affected by three structural factors. The first is the basic skeleton structure formed by graphene flakes, such as honeycomb-like [9], randomly-oriented [18], layered [19], and hierarchical [7] structures, etc. The second is the topological structures of CNT fibers intercalated into the GF matrix in a random [20] or ordered [21, 22] fashion. The last one is the connection between GFs and CNT additives through various forces [8, 18, 23] and geometrical configurations [9, 18].

Some effort has been made to study the relationship between the microstructures and mechanical properties of such a composite of CNTs and graphene sheets. Yang *et al* [24] experimentally speculated that CNTs could bridge adjacent graphene sheets and effectively inhibit the unfavorable aggregation of neighbor graphene sheets. In turn, Ye *et al* [25] found that graphene sheets have strong adsorption of CNT fibers and can suppress their aggregations as well. Kuang *et al* [9] fabricated the composite foam with long and entangled CNT fibers to weave graphene sheets into a continuous structure, which has an updated specific strength, elasticity and mechanical stability under compression compared with the pure CCGFs. Vinod *et al* [26] pointed out that the foam's mechanical failure is highly related to the vertical graphene cell walls, which could be strengthened by CNTs. Sun *et al* [18] and Guo *et al* [7] found that the compressive and tensile elasticities of GFs can be significantly enhanced through CNTs' addition due to the intensive recovery capacity of graphene cell walls reinforced by CNTs.

The CNT coated graphene flake, termed 'rebar graphene' by Tour *et al* [8, 20, 27], is one of the most typical structures [18–21, 27–29], which look like the vein-membrane structure of leaves and the wing of insects. However, the microscopic deformation mechanism of how this interesting composite structure strengthens the mechanical properties of the foam composites remains elusive, and it is still unclear how to choose parameters of CNTs and how to arrange them in GFs for the optimal design. In the present work, based on the previous experimental studies, a mesoscopic model of CCGF is established to systematically study the microscopic deformation mechanism and main influencing factors. Two main enhancing mechanisms of CNTs are finally found, i.e. the bar reinforcing mechanism, in which CNTs increase the bending stiffness of graphene flakes, and the mechanical locking mechanism, in which CNTs impede the relative sliding of adjacent graphene flakes. The rest of this paper is organized as follows. The numerical model of CCGF is introduced in the first part. The macroscopic mechanical behavior and microscopic deformation mechanism of CCGF under uniaxial compression are then studied as well as the feature of internal strain distribution, during which the foams made of CNTs and graphene flakes with different stiffness are considered. The effects of CNT fraction, distribution of CNTs on graphene flakes, the thickness of graphene flakes, and the adhesion strength between CNTs and graphene flakes on the initial and intermediate moduli of foam materials are finally studied. Conclusions are given at the end of this paper.

2. Numerical model and methodology

Based on the well proved coarse-grained models of CNT and graphene [30–32], we establish a coarse-grained mesoscopic model of CCGF material. For the graphene in the mesoscopic model, each bead represents a single- or multilayer atomic graphene sheet with an area of 2.5×2.5 nm^2. The stretching, shearing, and bending deformation of a graphene sheet and the van der Waals interaction between neighboring graphene sheets can be described by three harmonic and a Lennard-Jones (LJ) potential functions. (I) The energy of the tensile deformation of graphene sheets is described utilizing a harmonic spring potential $\phi_{gt} = k_{gt}(r_g - r_{g0})^2/2$ between all bonded coarse grains with an equilibrium distance of $r_{g0} = 2.5$ nm, where k_{gt} and r_g denote the spring constant and the current bead-to-bead distance, respectively; (II) the energy of the in-plane shear deformation is described using a harmonic rotational-spring potential $\phi_{g\varphi} = k_{g\varphi}(\varphi_g - \varphi_{g0})^2/2$ among three particles with a referenced equilibrium angle of $\varphi_{g0} = 90°$, in which $k_{g\varphi}$ and φ_g denote the spring constant and the current in-plane shear angle; (III) the energy of the out-of-plane bending deformation is described using a harmonic rotational-spring potential $\phi_{g\theta} = k_{g\theta}(\theta_g - \theta_{g0})^2/2$ among three particles with a referenced equilibrium angle of $\theta_{g0} = 180°$, in which $k_{g\theta}$ and θ_g are the spring constant and the current out-of-plane bending angle; (IV) the van der Waals interaction between neighbor coarse-grained flakes is described using the LJ potential function $\phi_{LJg} = 4\varepsilon_g[(\sigma_g/r_g)^{12} - (\sigma_g/r_g)^6]$, where ε_g, σ_g and r_g are the energy well depth, the zero-energy distance and the bead-to-bead distance.

For the CNT in the coarse-grained mesoscopic model, each bead represents a double-walled CNT with a length of 2 nm, chirality (8, 8) and (12, 12). A harmonic spring potential $\phi_{ct} = k_{ct}(r_c - r_{c0})^2/2$ and a harmonic rotational-spring potential $\phi_{c\theta} = k_{c\theta}(\theta_c - \theta_{c0})^2/2$ are used to describe the stretching and bending deformation of CNT, respectively. Here, k_{ct} and $k_{c\theta}$ are the spring constants for stretching and bending deformation, respectively. r_c is the current distance and r_{c0} is the equilibrium distance of 2 nm between neighboring beads. θ_c is the current angle and θ_0 denotes the equilibrium angle of $180°$ among three beads. The LJ potential $\phi_{LJc} = 4\varepsilon_c[(\sigma_c/r_c)^{12} - (\sigma_c/r_c)^6]$ is used to describe the interaction between two neighboring CNTs, where ε_c, σ_c, and r_c are the depth of the potential well, the zero-potential distance, and the current distance between neighboring beads. The interface interaction between the beads of graphene and the beads of CNTs is described by an LJ potential

Table 1. The force field parameters for the coarse-grained model from [30–32].

Parameters	Numbers of graphene layers				Units
	1	2	4	8	
k_{gt}	470	940	1860	3720	Kcal mol^{-1} Å^{-2}
$k_{g\varphi}$	16 870	33 740	67 480	134 960	Kcal mol^{-1} rad^{-2}
$k_{g\theta}$	144.9	8970	82 731	933 087	Kcal mol^{-1} rad^{-2}

Parameters	Value	Units	Parameters	Value	Units
k_{ct}	1880	Kcal mol^{-1} Å^{-2}	$k_{c\theta}$	90 000	Kcal mol^{-1} rad^{-2}
ε_g	473	Kcal mol^{-1}	σ_g	23.84	Å
ε_c	43.2	Kcal mol^{-1}	σ_c	19.7	Å

$\phi_{LJcg} = 4\varepsilon_{cg}[(\sigma_{cg}/r_{cg})^{12} - (\sigma_{cg}/r_{cg})^6]$, where $\varepsilon_{cg} = \varepsilon_g$ and $\sigma_{cg} = \sigma_g$ are adopted if not stated specifically. All parameters are given in table 1.

Such a coarse-grained model has been proved to be effective to describe the large deformation behaviors of graphene and CNT, for examples, the folding of graphene sheets [31], the torsion of graphene ribbons [32], the tension and compression of GFs composed of graphene sheets [33], the nano-indentation of CNT films [34], and the tension of CNT foams [35]. In the present work, all local strain of bonds in graphene sheets and CNTs is less than 10%, which ensures the validity of the linear constitutive relationship given above.

Periodic boundary conditions are used in all three directions of the mesoscopic model. Uniaxial compression is loaded in the *x*-direction with a strain rate of $\sim 10^7$ s^{-1}. Condition of the Langevin thermostat 300 K is adopted in all simulations with a time step 1 fs, and Berendsen barostat 0 Pa in the other two directions is adopted. All simulations are implemented with an open-source software Large-scale Atomic/Molecular Massively Parallel Simulator [36], and all figures and movies are illustrated using the open-source software Ovito [37].

A well-equilibrated coarse-grained model of CCGF is shown in figure 1(a), which consists of 100 CNT-coated graphene flakes. CNTs are colored blue and graphene flakes are colored red, respectively, as shown in figure 1(b-I). According to the coarse-grain scheme [9, 38], each CNT bead denotes a double-walled CNT with a length of 2 nm and chirality (8, 8) and (12, 12) as shown in figure 1(b-II). Each square coarse-grained graphene flake with a side length of 75 nm contains 961 beads and each bead denotes a square full-atomic graphene sheet with a side of 2.5 nm as shown in figure 1(b-III). Fourteen coarse-grained CNTs with an average length of $\sim$70 nm are tightly attached to the graphene flake in accordance with the experimental observation [18] shown in figure 1(b-IV). The density of the well-equilibrated coarse-grained model of CCGF is $\sim$60 mg cm^{-3}, which is consistent well with the range of 1–100 mg cm^{-3} measured experimentally [18, 39]. Four typical microstructures are identified in the simulation model as shown in figure 1(c(I–IV)), i.e. point–surface, edge–surface, edge–edge, and surface–surface contact, all of which have been identified in SEM

observations [7, 18, 19] as illustrated in figure 1(c) for comparison.

3. Results and discussion

3.1. The stress–strain relationship of CCGFs under uniaxial compression

In order to evaluate the effect of CNTs on the mechanical behavior of CCGF under compression, pure GFs with a corresponding similar graphene skeleton are also studied for comparison. Considering graphene flakes in real materials always contain 1–10 graphene layers [40], graphene flakes composed of 1-, 2-, 4-, and 8-layered graphene sheets are respectively adopted to evaluate the effect of graphene layers in the following text. The stress–strain relationships under uniaxial compression for pure GF and CCGF are shown in figure 2(a-I), both of which are composed of 1-layered graphene sheets. A typical rubber-like stress–strain relationship of both materials can be found, which can be divided into three stages, i.e. the initially elastic stage, the intermediate stage, and the final compaction stage. Both the pure GF and CCGF exhibit linear elasticity when the compressive strain is smaller than 0.01. Then, the compressive stress increases slightly until the strain reaches about 0.6. Finally, the stress increases sharply again when the compressive strain is larger than 0.6. Several typical snapshots and typical movies are given in figure 2(a(II, III)) and Movie S1–S2 (available online at stacks.iop.org/NANO/32/345704/mmedia) in supplementary data for an intuitive comparison. The rubber-like stress–strain relationships are qualitatively consistent with the experimental measurements for both the pure GF [17] and the CCGF [18]. Note that it is hard to quantitatively compare the present numerical results with those in experiments [9, 18], due to the size difference of graphene flakes in the numerical model and experimental samples, as well as the assumption of uniform-layered graphene flakes used in the numerical model, in compared with the non-uniform layered ones in a real material. Under the same strain, the stress of the CCGF is always larger than that of the pure GF as shown in figure 2(b). The initial elastic modulus E_{init} $(0 < \varepsilon < 0.01)$ and the intermediate modulus E_m $(0.01 < \varepsilon < 0.1)$ are extracted
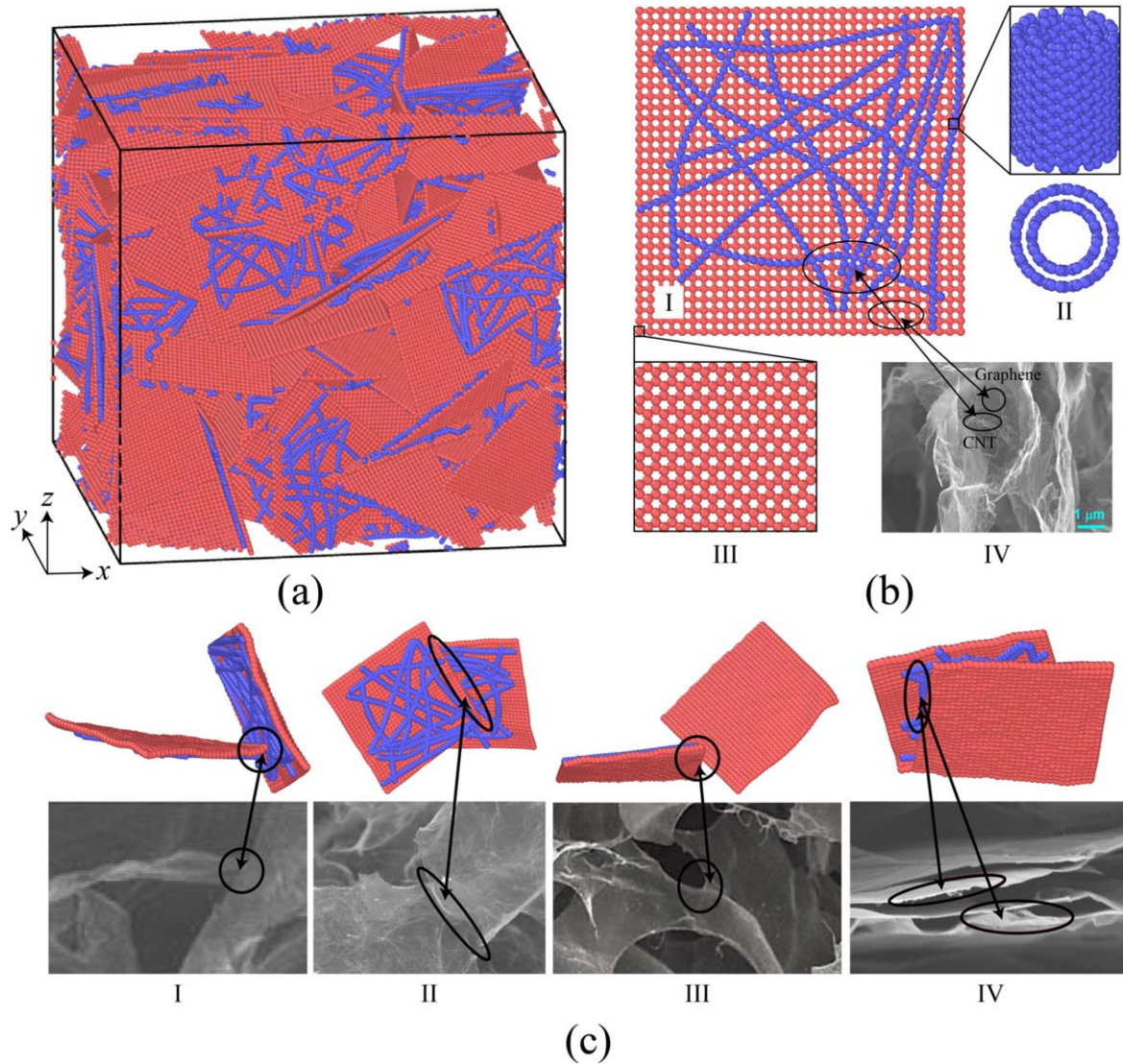
Figure 1. Schematics of the simulation model and the corresponding microstructures. (a) The coarse-grained model of CCGF. (b) The model of the constituents: I. The coarse-grained model of a CNT-coated graphene flake; II. A full-atomic double-walled CNT with a length of 2 nm, and chirality of (8,8) and (12,12); III. A full-atomic graphene sheet with a side length of 2.5 nm; IV. The SEM image of a CNT-coated graphene sheet observed in the experiment [18] John Wiley & Sons. Copyright © 2013 WILEY-VCH Verlag GmbH & Co. KGaA (c) Four kinds of contact microstructures: (I) the point–surface contact structures reported, reproduced from [7]. CC BY 4.0. (II) the edge–surface contact structures reported in [18]. John Wiley & Sons. Copyright © 2013 WILEY-VCH Verlag GmbH & Co. KGaA, Weinheim; (III) the edge–edge contact structures reported in [18]. John Wiley & Sons. Copyright © 2013 WILEY-VCH Verlag GmbH & Co. KGaA, Weinheim; (IV) the surface–surface contact structures reported, reprinted from [19], Copyright (2018), with permission from Elsevier.

from the stress–strain curves as shown in figure 2(c), where it shows that both initial and intermediate moduli increase with the increase of graphene layers and both moduli of CCGF are always larger than those of the corresponding pure GF. For example, the modulus of the CCGF composed of 1-layered graphene sheets almost equals that of the pure GF composed of 4-layered graphene sheets. Such an enhancing effect is well consistent with the experimental measurement that the modulus of CNT/graphene composite is almost twice that of the pure GF [9]. Note that the intermediate modulus is smaller than the initial modulus, which is due to the rearrangement of graphene flakes under relatively large compressive strain [33]. Therefore, the addition of CNT is an effective method to raise the modulus of GF.

3.2. The microscopic deformation mechanism of CCGFs

Two microscopic deformation mechanisms are found from plenty of calculations, which are shown in figure 3. The bar reinforcing mechanism dominates the microstructural deformation in CCGFs composed of relatively soft graphene flakes, while the mechanical locking mechanism dominates the microstructural deformation of CCGFs composed of relatively stiff graphene flakes. As an example shown in figure 3(a), the snapshots denote the deformation of a soft 1-layered graphene flake in the pure GF and the CCGF composed of 1-layered graphene flakes, respectively. One can see that, under the same strain, the 1-layered graphene flake in the pure GF rolls into a mass like a piece of gauze scarf, while the deformation of CNT reinforced 1-layered graphene flake
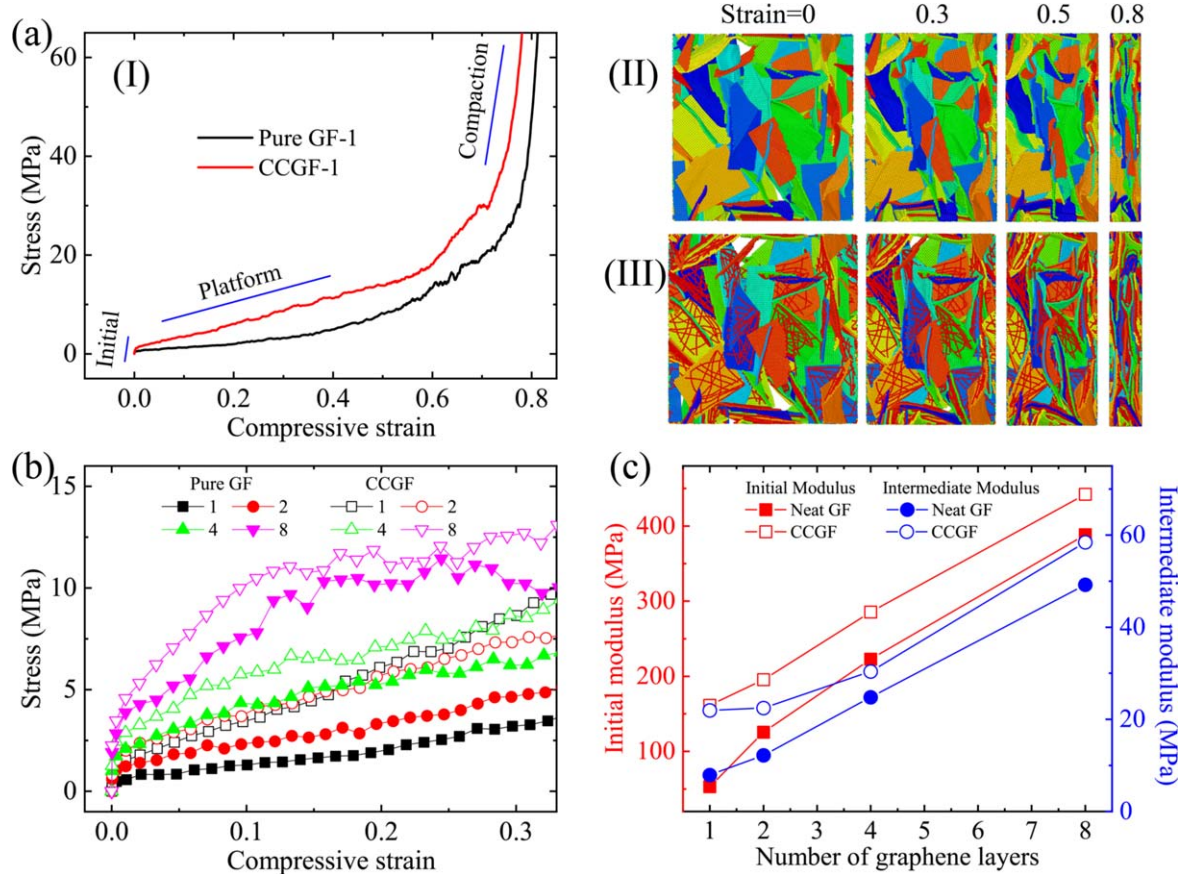
Figure 2. The stress–strain relationships, moduli, and typical snapshots for pure GF and CCGF. (a-I) The stress–strain response of CCGF composed of 1-layered graphene sheet under uniaxial compression and pure GF; (a-II) typical snapshots of pure GF under uniaxial compression with different strain values; (a-III) typical snapshots of CCGF composed of 1-layered graphene sheet under uniaxial compression with different strain values; (b) the stress–strain relationships of CCGF composed of 1-, 2-, 4- and 8-layered graphene sheets, where those of pure GF composed of 1-, 2-, 4- and 8-layered graphene sheets are given for comparison; (c) the initial and intermediate moduli of pure GF and CCGF varying with the layer of graphene sheets. The flakes in the snapshots are labeled in different colors.

is hugely restrained. The CNT-coated 1-layered graphene flake has a similar structure with the vein-strengthened membrane of leaves [21], in which the bending stiffness of CNT (double-walled CNT used in the present paper) is much larger than 1-layered graphene but almost the same as that of 4-layered graphene as shown in figure S1. Therefore, the bending stiffness of the CNT-coated 1-layered graphene flake is much close to that of the CNT, and comparable with that of the 4-layered graphene sheet. In addition, it is well known that the stiffness of graphene sheets increases with the increase of their layers, which will subsequently increase the modulus of the corresponding GF. In a pure GF composed of relatively stiff graphene flakes, the neighboring contacting flakes are much easier to slide against each other [33, 41]. However, in CCGFs composed of relatively stiff graphene flakes, the sliding behavior is significantly hindered and replaced by a locking behavior due to the restriction of CNT networks, which further enhances the loading capability and increases the modulus of CCGFs. Typical snapshots are shown in figure 3(b), where the sliding behavior is obvious in pure GFs composed of relatively stiff graphene flakes, while the locking behavior is significant in CCGFs composed of relatively stiff graphene flakes. Such a mechanical locking

mechanism can also be induced in pure GFs composed of hole-graphene flakes [42, 43], where the movement of flakes is locked by the hole. It should be noted that the two enhancing mechanisms would work simultaneously either in a CCGF composed of soft graphene flakes or in that composed of stiff ones, especially for a real CCGF that consists of both soft and stiff graphene flakes.

3.3. The microscopic deformation field in CCGFs

In the pure GF and CCGF composed of 1-layered graphene flakes, initially, negligible stress exists in the graphene flakes in either GF or CGGF, as most beads are shown in green in figures 4(a) and (b) at a vanishing strain. However, both compressive and tensile stresses exist in the CNTs in CCGF, as indicated in red and blue in figure 4(b), which should be induced by the entanglement of CNTs. With the increase of compressive strain, the local stress becomes more nonuniform in the pure GF. Both negative local stress of ~-9 GPa and positive stress of ~5 GPa coexist in the same graphene flake due to its dramatic nonuniform deformation at the compressive strain of 0.8, which can be found in the snapshot of the flake in figure 4(a). However, the stress state of the graphene
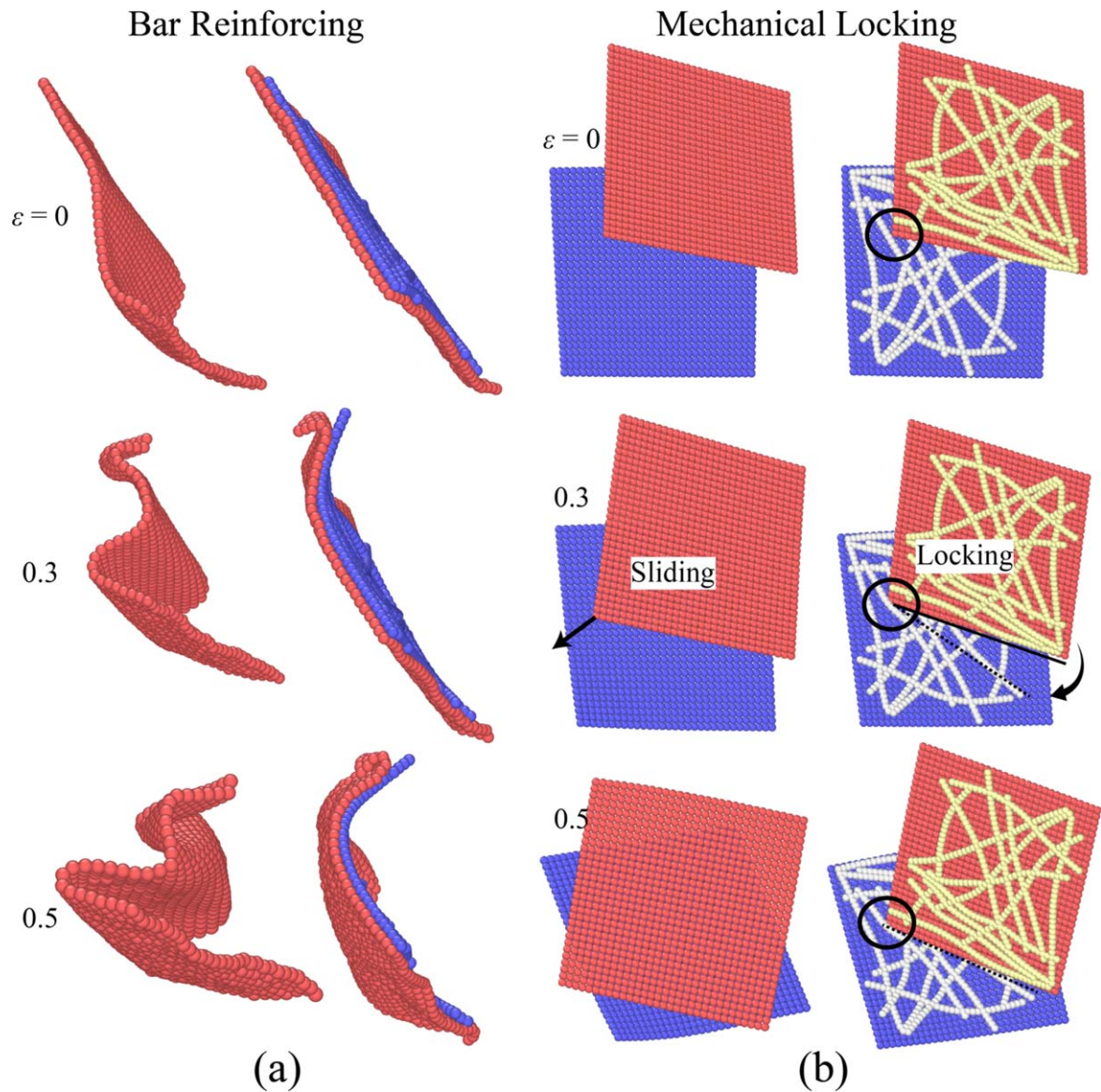
Figure 3. Typical snapshots of microstructural deformation in different CCGFs under different strains. (a) The bar reinforcing mechanism in CCGF composed of 1-layered graphene flakes; (b) the mechanical locking mechanism in CCGF composed of 8-layered graphene flakes.

flakes in CCGF remains almost unchanged with the increase of the compressive strain, but the stress in the CNTs in CCGF changes drastically. For example, the local stress in CNTs is about 8 GPa as marked by a black circle, then decreases to $\sim$2.5 GPa as the strain increases to 0.5, and finally decreases to a negative value ~-2.8 GPa. It can be inferred that CNTs in the 1-layered graphene flakes act as reinforcing bars to strengthen the graphene skeleton. In comparison, the stress distribution in CCGF composed of relatively stiff graphene flakes, for example, that of 8-layered graphene flakes as shown in figures 4(c) and (d), is much different from the stress state in CCGF composed of relatively soft graphene flakes. Local stress concentration emerges in a small part of graphene flakes and the stress distribution in CNTs is almost unchanged with the increase of compressive strain, which can be found from the snapshots in figure 4(d). It demonstrates that the external load is transmitted mainly through stiff graphene flakes in this case. Here, we noted that the

maximum strain in the CNT and graphene sheets in figure 4(d) is 4.3%, smaller than the limited strain of 10% [32], which ensures the effectiveness of the linear constitutive relationship mentioned in section 2, i.e. the 'Numerical model and methodology' section.

3.4. The influencing factors affecting the compression properties of CCGFs

The volume fraction and arrangement of CNTs in CCGFs can be tuned by different preparation technologies, such as chemical vapor deposition [21], 3D printing [44], sol-cryo [18]. Figures 5(a) and (b) give the effect of the volume fraction and three kinds of arrangements of CNTs (see the insets in figure 5(a)) on the modulus of CCGFs composed of relatively soft graphene flakes. No matter what kind of arrangement of CNTs, both the initial and intermediate moduli of CCGFs are enhanced with increasing CNT volume fraction, qualitatively
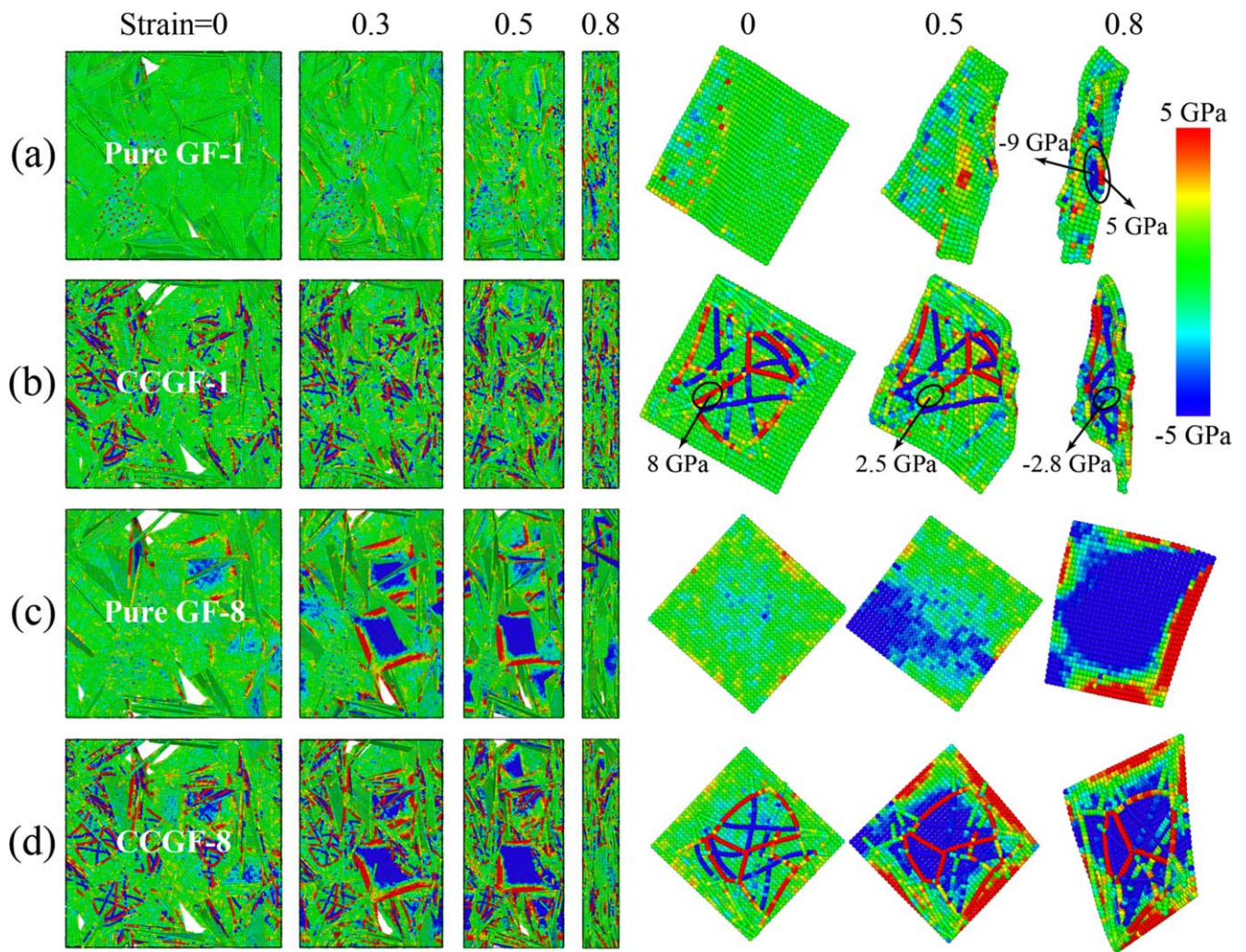
Figure 4. The local stress distributions in pure GF and CCGF, both of which are composed of 1-layered (a), (b) and 8-layered (c), (d) graphene flakes.

consistent with the experiment results [9, 18], Besides, the intermediate moduli of foams composed of parallel CNTs are a little smaller than those of foams containing randomly or orthogonally arranged CNTs, especially when the strain is larger than 0.25, which can be well explained by the microscopic deformation shown in figure 5(c). CNT-coated graphene flakes with random and orthogonal structures under horizontal compression would remain flat even at a strain of 0.5, while the flake with parallel ones has obvious out-of-plane bending deformation at a strain of 0.3. That is to say, randomly and orthogonally distributed CNT networks can enhance the bending stiffness of flakes in many directions, while the stiffness of flakes with parallel CNTs can be significantly enhanced only in the direction of CNTs. As a result, the CNT-coated graphene flakes will be bent in a particular direction that is easier to bend, as shown in figure 5(c). As we know from figure S1 in supplementary data, the bending stiffness of 4-layered graphene flakes is close to that of the present adopted double-walled CNTs. For the foam composed of 8-layered graphene flakes, one can see that both the initial and intermediate moduli are slightly influenced by the volume fraction and arrangement of CNTs

as shown in figure S4 in supplementary data. This is because the bending stiffness of double-walled CNTs is much smaller than the stiff 8-layered graphene flake (figure S2), the change in volume fraction and arrangement of CNTs has negligible effects on the out-of-plane bending deformation of stiff graphene flakes, and weakly influence the modulus of CCGF composed of stiff graphene flakes. If one wants to enhance the modulus of GFs composed of stiff graphene flakes, one way is to use harder reinforcements and another way is to add cross-links or use long CNT to connect neighboring graphene flakes. The cross-links or long CNTs will weave graphene flakes into a continuous structure [9].

Since the adhesion strength between CNTs and graphene flakes may be affected by several factors such as van der Waals force [9, 18], π–π [23] or covalent bonding [8, 20], figure 6 further shows the effect of adhesion strength between CNTs and graphene flakes on the mechanical behavior of CCGFs. The relative adhesion strength λ, i.e. the ratio of the adhesion strength of the CNT-graphene interface to that of the graphene–graphene interface, is tuned in a wide range of (0.01, 2). In our simulations, an LJ potential function $\phi_{\mathrm{LJcg}} = 4\varepsilon_{\mathrm{cg}}[(\sigma_{\mathrm{cg}}/r_{\mathrm{cg}})^{12} - (\sigma_{\mathrm{cg}}/r_{\mathrm{cg}})^{6}]$ is adopted to depict the
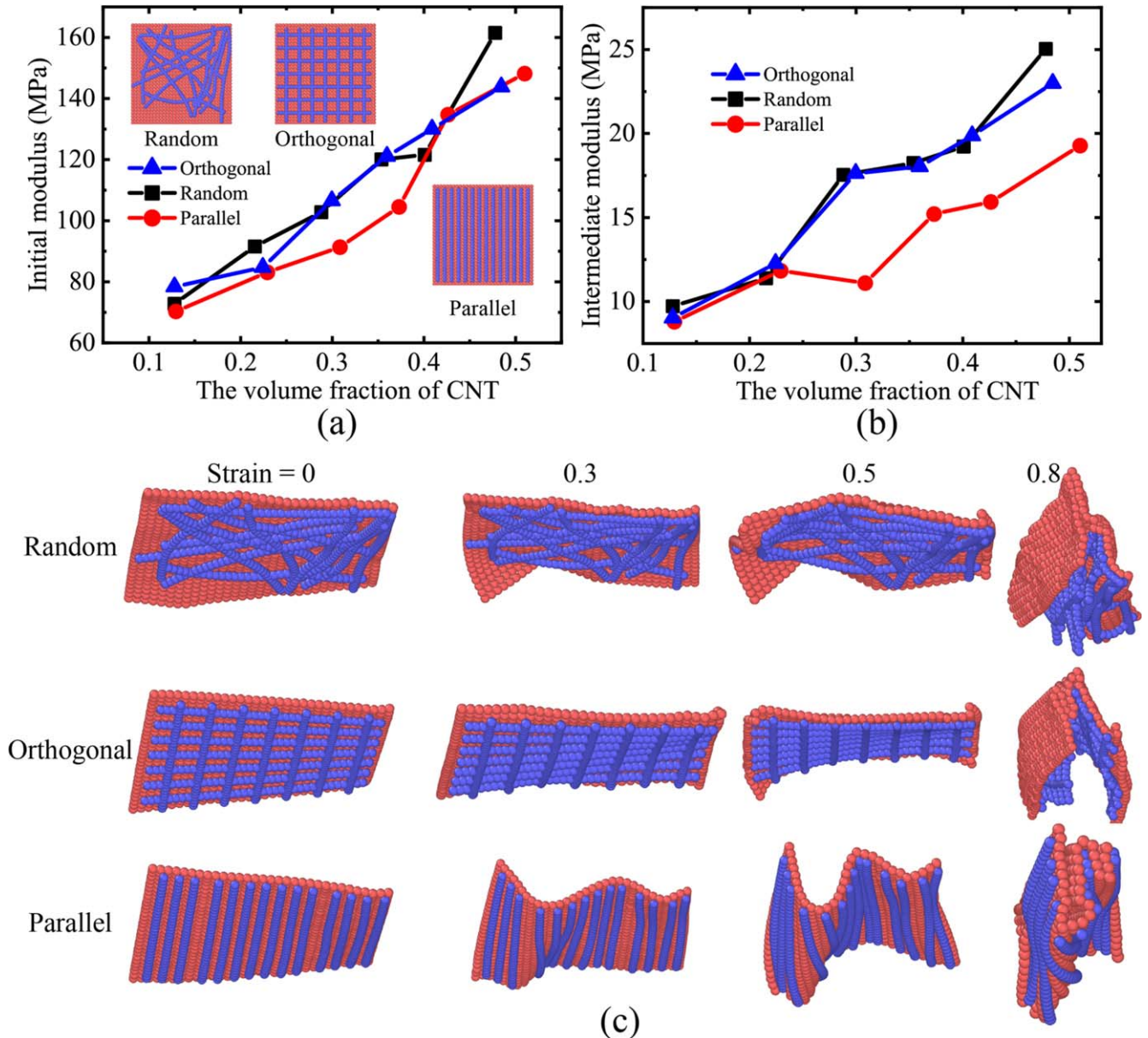
Figure 5. The effect of the volume fraction and arrangement of CNTs in CCGFs composed of relatively soft graphene flakes. (a) Initial modulus of the CCGFs with varied volume fraction and arrangement of CNTs; (b) intermediate modulus of CCGFs with varied volume fraction and arrangement of CNTs; (c) snapshots of typical CNT-coated graphene sheets with different CNT arrangements.

adhesion strength between CNTs and graphene flakes, in which the depth of the potential well ε_{cg} determines the adhesion strength. It is well known that in experiments, the interfacial strength between CNTs and graphene flakes should be influenced by different experimental techniques. In order to be comparable with such an experimental phenomenon, we introduce a dimensionless interfacial adhesion strength λ with the definition of $\lambda = \varepsilon_{cg}/\varepsilon_g$, in which ε_{cg} and ε_g denote respectively the energy well depth in the LJ potential functions of the CNT-graphene interaction and graphene–graphene interaction. The parameter ε_g is set as a constant, while ε_{cg} varies in a range, representing the different interfacial adhesion strength between the CNT and graphene flake. It shows that both the initial and intermediate moduli increase with the increase of λ as shown in figure 6(a). In the case with

a weak adhesion strength $\lambda = 0.01$, graphene flakes can be deformed continuously under compression due to the easy decohesion of the CNT-graphene interface as shown in figure 6(b). When the relative adhesion strength achieves about 0.5, decohesion between CNTs and graphene flakes may not happen as shown in figure 6(c).

4. Conclusions

Based on the coarse-grained molecular dynamics method, numerical experiments are systematically carried out to reveal the microscopic deformation mechanism and study the main influencing factors of CCGFs under uniaxial compression. Two microscopic deformation mechanisms are observed, i.e.
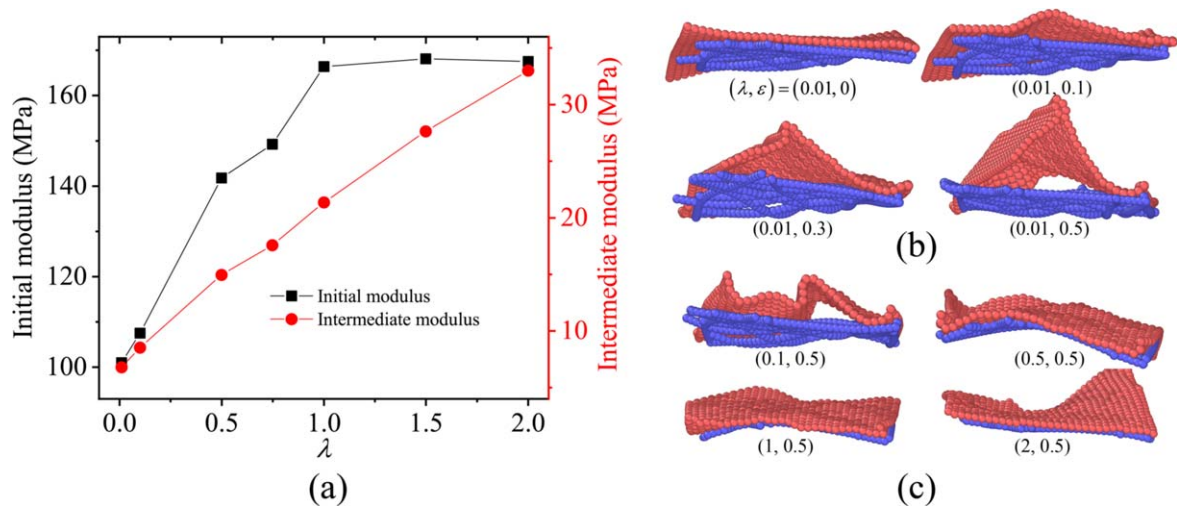
Figure 6. The effect of adhesion strength between CNTs and graphene flakes on the modulus of CCGFs under compression. (a) The initial and intermediate moduli of CCGFs with various relative adhesion strength, $\lambda = \varepsilon_{gc}/\varepsilon_g$, where ε_{gc} is the depth of the potential well for CNT-graphene interaction, where ε_g is the depth of the potential well for graphene beads. (b) Typical snapshots for CNT-coated graphene flakes with various compressive strain $\varepsilon = 0, 0.1, 0.3, 0.5$ at a given $\lambda = 0.01$. (c) Typical snapshots for CNT-coated graphene sheet with various adhesion strength $\lambda = 0.1, 0.5, 1, 2$ at $\varepsilon = 0.5$.

the bar reinforcing mechanism and the mechanical locking mechanism, which dominates the microscopic deformation of CCGFs composed of relatively soft and stiff graphene flakes, respectively. It is found that the CNT acts as a reinforcing bar, enhancing the deformation capacity of relatively soft graphene flakes and further increasing the modulus of CCGFs. In CCGFs composed of relatively stiff graphene flakes, the CNT acts as a mechanical lock, inhibiting the point–surface sliding between neighboring flakes and increasing the modulus of foams. The nonuniformity of local stress and deformation energy distributions in CCGFs increases with the increase of compressive strain, resulting in a highly nonuniform microscopic deformation of CCGFs. Both the initial compressive modulus and the intermediate one of CCGFs increase significantly with the increase of thickness of graphene flakes, volume fraction of CNTs, and the adhesion strength between CNTs and graphene flakes. The modulus of CCGFs with parallelly-arranged CNTs is smaller than that of CCGFs with randomly or orthogonally-arranged CNTs. The results of this paper are helpful to understand the mechanical properties of CNT-graphene hybrid materials and to optimize the design of advanced graphene-based composite materials.

5. Methods

5.1. Fabrication of numerical samples

To construct the initial configuration of such a GF system, 100 CNT-coated graphene flakes (figure 1(b1)) are placed randomly in a big cubic box to ensure no interaction among each other. Then, the isothermal–isobaric ensemble (NPT) technique is adopted to make the system shrink with a periodic boundary condition in three directions as well as a constant temperature of 300 K and one barometric pressure. The system is then fully relaxed for 10 ns to reach an equilibrium state with the time step 1 fs. After the relaxation, the final configuration shown in figure 1(a) is obtained, in which CNT-coated graphene flakes are randomly oriented.

5.2. The local state of stress

The virial stress is always viewed as a measure of mechanical stress in micro/mesoscale, the virial stress on atom i can be achieved according to $\sigma_{XX} = \frac{1}{V}\sum_i \frac{1}{2}\sum_{j=1}^{N}(R_X^j - R_X^i)F_X^{ij} + m^i v_X^i v_X^i$, in which V is the volume of one atom, R_X^α and R_X^β denote the positions of atoms α and β in X-axis. $F_X^{\alpha\beta}$ is the force acted on atom i induced by atom j in the X direction, m^i is the mass of atoms i, v_X^i is the velocity of atom i in the X-axis.

Data availability statement

All data that support the findings of this study are included within the article (and any supplementary files).

Notes

There are no conflicts of interest to declare.

Author contributions

S H C and C W conceived the original idea, designed, and supervised the simulations. S W formulated the numerical model, conducted all simulations, and drafted the paper. C W and S H C revised the manuscript. All authors reviewed and contributed to the paper.

ORCID iDs

Shuai Wang ⬤ https://orcid.org/0000-0001-5569-7157
Chao Wang ⬤ https://orcid.org/0000-0002-3234-6917
Muhammad Bilal Khan ⬤ https://orcid.org/0000-0002-8316-3002
Shaohua Chen ⬤ https://orcid.org/0000-0002-5277-453X

References

[1] Iijima S 1991 Helical microtubules of graphitic carbon *Nature* **354** 56–8

[2] Novoselov K S, Geim A K, Morozov S V, Jiang D, Zhang Y, Dubonos S V, Grigorieva I V and Firsov A A 2004 Electric field effect in atomically thin carbon films *Science* **306** 666–9

[3] Novoselov K S, Fal'ko V I, Colombo L, Gellert P R, Schwab M G and Kim K 2012 A roadmap for graphene *Nature* **490** 192–200

[4] Peng B, Locascio M, Zapol P, Li S, Mielke S L, Schatz G C and Espinosa H D 2008 Measurements of near-ultimate strength for multiwalled carbon nanotubes and irradiation-induced crosslinking improvements *Nat. Nanotechnol.* **3** 626–31

[5] Lu Z, Foroughi J, Wang C, Long H and Wallace G G 2018 Superelastic hybrid CNT/Graphene fibers for wearable energy storage *Adv. Energy Mater.* **8** 1702047

[6] Ma J, Wang P, Chen H, Bao S, Chen W and Lu H 2019 Highly sensitive and large-range strain sensor with a self-compensated two-order structure for human motion detection *ACS Appl. Mater. Interfaces* **11** 8527–36

[7] Guo F, Jiang Y, Xu Z, Xiao Y, Fang B, Liu Y, Gao W, Zhao P, Wang H and Gao C 2018 Highly stretchable carbon aerogels *Nat. Commun.* **9** 881

[8] Sha J *et al* 2017 Three-dimensional rebar graphene *ACS Appl. Mater. Interfaces* **9** 7376–84

[9] Kuang J, Dai Z, Liu L, Yang Z, Jin M and Zhang Z 2015 Synergistic effects from graphene and carbon nanotubes endow ordered hierarchical structure foams with a combination of compressibility, super-elasticity and stability and potential application as pressure sensors *Nanoscale* **7** 9252–60

[10] Yu D, Goh K, Wang H, Wei L, Jiang W, Zhang Q, Dai L and Chen Y 2014 Scalable synthesis of hierarchically structured carbon nanotube–graphene fibres for capacitive energy storage *Nat. Nanotechnol.* **9** 555–62

[11] Kausar A 2019 Advances in polymer-anchored carbon nanotube foam: a review *Polym.—Plast. Technol. Mater.* **58** 1965–78

[12] You R, Liu Y Q, Hao Y L, Han D D, Zhang Y L and You Z 2020 Laser fabrication of graphene-based flexible electronics *Adv. Mater.* **32** 1901981

[13] Luo S, Samad Y A, Chan V and Liao K 2019 Cellular graphene: fabrication, mechanical properties, and strain-sensing applications *Matter* **1** 1148–202

[14] Qin S, Liu Y, Jiang H, Xu Y, Shi Y, Zhang R and Wang F 2019 All-carbon hybrids for high-performance electronics, optoelectronics and energy storage *Sci. China Inf. Sci.* **62** 220403

[15] Senthil Kumar K, Chen P-Y and Ren H 2019 A review of printable flexible and stretchable tactile sensors *Research* **2019** 1–32

[16] Wu Z, Wang Y, Liu X, Lv C, Li Y, Wei D and Liu Z 2019 Carbon-nanomaterial-based flexible batteries for wearable electronics *Adv. Mater.* **31** 1800716

[17] Wu Y *et al* 2015 Three-dimensionally bonded spongy graphene material with super compressive elasticity and near-zero Poisson's ratio *Nat. Commun.* **6** 6141

[18] Sun H, Xu Z and Gao C 2013 Multifunctional, ultra-flyweight, synergistically assembled carbon aerogels *Adv. Mater.* **25** 2554–60

[19] Zhou E, Xi J, Guo Y, Liu Y, Xu Z, Peng L, Gao W, Ying J, Chen Z and Gao C 2018 Synergistic effect of graphene and carbon nanotube for high-performance electromagnetic interference shielding films *Carbon* **133** 316–22

[20] Yan Z *et al* 2014 Rebar graphene *ACS Nano* **8** 5061–8

[21] Lin X, Liu P, Wei Y, Li Q, Wang J, Wu Y, Feng C, Zhang L, Fan S and Jiang K 2013 Development of an ultra-thin film comprised of a graphene membrane and carbon nanotube vein support *Nat. Commun.* **4** 2920

[22] Hu D, Gong W, Di J, Li D, Li R, Lu W, Gu B, Sun B and Li Q 2017 Strong graphene-interlayered carbon nanotube films with high thermal conductivity *Carbon* **118** 659–65

[23] Chen X, Tao J, Yi J, Liu Y, Li C and Bao R 2018 Strengthening behavior of carbon nanotube-graphene hybrids in copper matrix composites *Mater. Sci. Eng.* A **718** 427–36

[24] Yang S-Y, Lin W-N, Huang Y-L, Tien H-W, Wang J-Y, Ma C-C M, Li S-M and Wang Y-S 2011 Synergetic effects of graphene platelets and carbon nanotubes on the mechanical and thermal properties of epoxy composites *Carbon* **49** 793–803

[25] Ye M, Hu C, Lv L and Qu L 2016 Graphene-winged carbon nanotubes as high-performance lithium-ion batteries anode with super-long cycle life *J. Power Sources* **305** 106–14

[26] Vinod S, Tiwary C S, Machado L D, Ozden S, Vajtai R, Galvao D S and Ajayan P M 2016 Synthesis of ultralow density 3D graphene–CNT foams using a two-step method *Nanoscale* **8** 15857–63

[27] Hacopian E F, Yang Y, Ni B, Li Y, Li X, Chen Q, Guo H, Tour J M, Gao H and Lou J 2018 Toughening graphene by integrating carbon nanotubes *ACS Nano* **12** 7901–10

[28] Liu Y, Liu Y, Qin S, Xu Y, Zhang R and Wang F 2017 Graphene-carbon nanotube hybrid films for high-performance flexible photodetectors *Nano Res.* **10** 1880–7

[29] Maarouf A A, Kasry A, Chandra B and Martyna G J 2016 A graphene–carbon nanotube hybrid material for photovoltaic applications *Carbon* **102** 74–80

[30] Cranford S, Yao H, Ortiz C and Buehler M J 2010 A single degree of freedom 'lollipop' model for carbon nanotube bundle formation *J. Mech. Phys. Solids* **58** 409–27

[31] Cranford S, Sen D and Buehler M J 2009 Meso-origami: folding multilayer graphene sheets *Appl. Phys. Lett.* **95** 225502

[32] Cranford S and Buehler M J 2011 Twisted and coiled ultralong multilayer graphene ribbons *Modelling Simul. Mater. Sci.* **19** 054003

[33] Wang C, Zhang C and Chen S 2016 The microscopic deformation mechanism of 3D graphene foam materials under uniaxial compression *Carbon* **109** 666–72

[34] Steven W C and Markus J B 2010 *In silico* assembly and nanomechanical characterization of carbon nanotube buckypaper *Nanotechnology* **21** 265706

[35] Xie B, Liu Y, Ding Y, Zheng Q and Xu Z 2011 Mechanics of carbon nanotube networks: microstructural evolution and optimal design *Soft Matter* **7** 10039–47

[36] Plimpton S 1995 Fast parallel algorithms for short-range molecular dynamics *J. Comput. Phys.* **117** 1–19

[37] Stukowski A 2009 Visualization and analysis of atomistic simulation data with OVITO–the open visualization tool *Modelling Simul. Mater. Sci.* **18** 015012

[38] Dai Z, Liu L, Qi X, Kuang J, Wei Y, Zhu H and Zhang Z 2016 Three-dimensional sponges with super mechanical stability: harnessing true elasticity of individual carbon nanotubes in macroscopic architectures *Sci. Rep.* **6** 18930

[39] Ma Z, Wei A, Ma J, Shao L, Jiang H, Dong D, Ji Z, Wang Q and Kang S 2018 Lightweight, compressible and electrically conductive polyurethane sponges coated with synergistic multiwalled carbon nanotubes and graphene for piezoresistive sensors *Nanoscale* **10** 7116–26

[40] Das S, Seelaboyina R, Verma V, Lahiri I, Hwang J Y, Banerjee R and Choi W 2011 Synthesis and characterization of self-organized multilayered graphene–carbon nanotube hybrid films *J. Mater. Chem.* **21** 7289–95

[41] Wang C, Zhang C and Chen S 2019 Micro-mechanism and influencing factors of graphene foam elasticity *Carbon* **148** 267–76

[42] Pan D, Wang C and Wang X 2018 Graphene foam: hole-flake network for uniaxial supercompression and recovery behavior *ACS Nano* **12** 11491–502

[43] Pan D, Wang C, Wang T-C and Yao Y 2017 Graphene foam: uniaxial tension behavior and fracture mode based on a mesoscopic model *ACS Nano* **11** 8988–97

[44] Peng M *et al* 2019 3D printing of ultralight biomimetic hierarchical graphene materials with exceptional stiffness and resilience *Adv. Mater.* **31** 1902930